Towards a theoretical understanding of multiscalar drought indices based on the relationship between precipitation and standardized precipitation index

Lin Wang, Gang Huang & Wen Chen

Theoretical and Applied Climatology

ISSN 0177-798X
Volume 136
Combined 3-4

Theor Appl Climatol (2019)
136:1465-1473
DOI 10.1007/s00704-018-2578-2

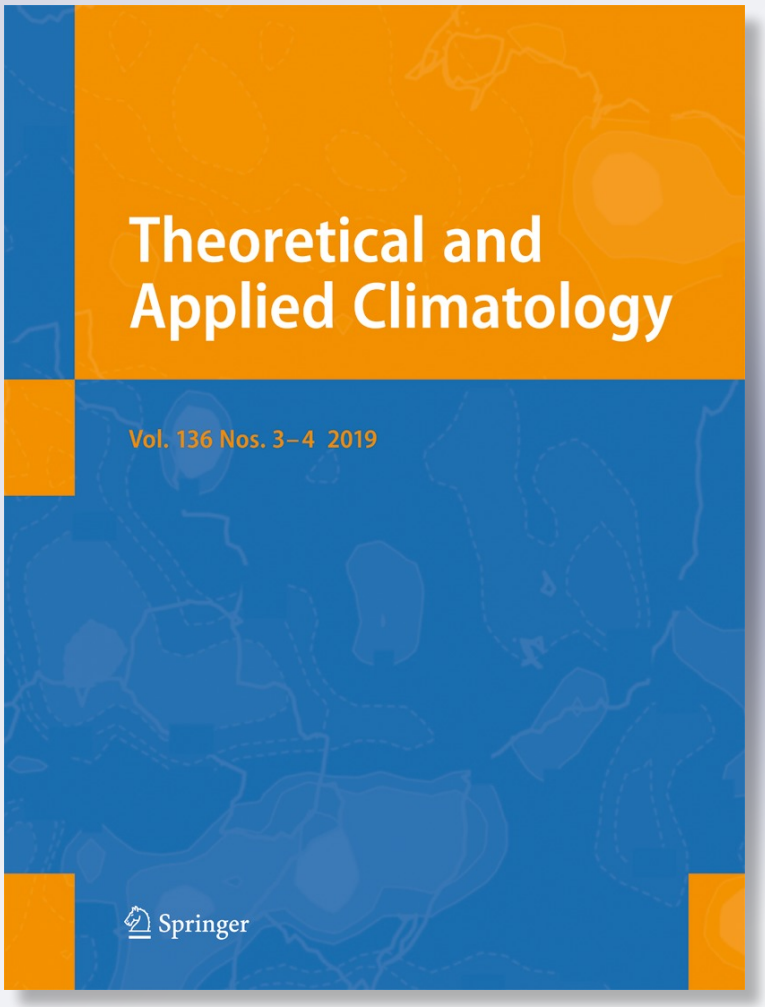

Springer

Theoretical and Applied Climatology (2019) 136:1465–1473
https://doi.org/10.1007/s00704-018-2578-2

ORIGINAL PAPER

Towards a theoretical understanding of multiscalar drought indices based on the relationship between precipitation and standardized precipitation index

Lin Wang [1,2] · Gang Huang [1,3] · Wen Chen [1,3,4]

Received: 21 February 2017 / Accepted: 24 July 2018 / Published online: 31 July 2018

Abstract
This study reports a theoretical understanding of multiscalar drought indices based on the relationship between precipitation and Standardized Precipitation Index (SPI). To unveil the multiscalar structure of precipitation, the advanced technique of wavelet decomposition is systematically applied to dissect the precipitation into a number of orthogonal components according to different time scales. A case study over Southwest China demonstrated a time lag or a synchronous correlation, depending on the time scale, between precipitation and the SPI, with precipitation always leading the SPI. The delayed response of the SPI to precipitation becomes more significant as the temporal scale increases, while the lead-lag effect vanishes at the shortest time scales. Most importantly, the SPI at a specific time responds primarily to the corresponding precipitation component, regardless of the contribution of its variance to the total variability. The conclusions obtained in the case study are further strengthened by global analysis. Moreover, the lag time between the SPI and precipitation at longer time scales has great geographic diversity worldwide, in contrast to shorter time scales, which have spatially uniform response times irrespective of site. In addition, we also clarify two core concepts that are easily confused, time scale and lag time. Finally, our study highlights the prominent utility of a multiscalar drought index to detect drought for a wide range of time scales compared to other metrics with rigid time scale, owing to the multistructural property of precipitation that results in multiscalar drought.

1 Introduction

Drought is the world's costliest natural disaster, causing tremendous economic losses annually and affecting more people than any other form of natural disaster (Wilhite 2000). Moreover, drought is among the most complex of climatic phenomena, mainly because it is difficult to quantify its severity, describe its spatial coverage, and pinpoint its beginning and end (Wilhite 2006). A drought index, which is synthetic information about wet and dry conditions, is central to the identification and quantification of drought phenomena and is especially indispensable for policy makers (Heim 2000). In past decades, various drought indices of varying complexity and algorithms have been developed in order to provide a quantitative and objective evaluation of drought (Heim 2002; Dai 2011a). The most popular drought indices with extensive application include the Palmer Drought Severity Index (PDSI) (Palmer 1965; Wells et al. 2004), the Standardized Precipitation Index (SPI) (McKee et al. 1993), and the Standardized Precipitation Evapotranspiration Index (SPEI) (Vicente-Serrano et al. 2010). The relationship among different drought indices has been extensively examined in previous studies. McKee et al. (1995) pointed out that the PDSI had the highest correlation to the SPI with a 10–14 month time scale for most individual stations in the USA; Guttman (1998) reached a similar conclusion. Recently, Vicente-Serrano et al. (2010) investigated the correlation between the PDSI and SPEI at different time scales globally and concluded that a high correlation was maintained at time scales of 12–

✉ Gang Huang
hg@mail.iap.ac.cn

[1] State Key Laboratory of Numerical Modeling for Atmospheric Sciences and Geophysical Fluid Dynamics, Institute of Atmospheric Physics, Chinese Academy of Sciences, P. O. Box 9804, Beijing 100029, China

[2] Plateau Atmosphere and Environment Key Laboratory of Sichuan Province, Chengdu, China

[3] University of Chinese Academy of Sciences, Beijing 100049, China

[4] Center for Monsoon System Research, Institute of Atmospheric Physics, Chinese Academy of Sciences, Beijing 100190, China

18 months. Vicente-Serrano et al. (2011a) found that the SSI (Standardized Streamflow Index) was highly correlated with both the SPEI and SPI at time scales of 3–8 months on the northwest Iberian Peninsula. McEvoy et al. (2012) evaluated two multiscalar drought indices, SPEI and SPI, and suggested that both indicators were remarkably correlated to surface water availability throughout Nevada and eastern California, with SPEI showing some advantage over SPI. Wang and Chen (2014) investigated the correlation between the PDSI and SPEI within China and suggested that how well the SPEI correlates with PDSI depends on the time scale: at a time scale of less than 10 months, a poor correlation is observed; at a time scale of greater than 10 months, the correlation coefficient between SPEI and PDSI remains between 0.7 and 0.9. In particular, Vicente-Serrano et al. (2012) provided a global assessment to compare different indices including the SPEI, SPI, and four versions of the PDSI.

However, the basic relationship between precipitation and drought indices is usually overlooked and poorly understood, though precipitation is usually a dominant variable in the formulation of a drought index. Consequently, the purpose of this study is to reveal the quantitative relationship between precipitation and drought indices. The SPI is chosen as a representative multiscalar drought index since it depends entirely on precipitation and ignores other variables. As we know, the SPI can be calculated at different temporal scales, enabling it to identify different types of drought. However, the multiscalar structure of precipitation is not apparent; towards this goal, the wavelet decomposition technique is applied to dissect the precipitation at different time scales. Despite the popularity of wavelet analysis in atmospheric science to determine the dominant period of a time series and how it varies with time (Meyers et al. 1993; Torrence and Compo 1998), wavelet decomposition is seldom used to decompose a time series into several components according to different time scales.

This paper is structured as follows: The mathematical principles of wavelet decomposition and the SPI are respectively introduced in Sections 3.1 and 3.2, after a brief description of data sources in Section 2. To provide an in-depth view, a detailed case study is presented in Section 4. Subsequently, the research scope is expanded to the global scale and discussed in Section 5. Finally, Section 6 is devoted to concluding remarks and further discussion. Southwest China, covering 22.25–31.75° N, 98.75–109.25° E, is chosen as the research case, since it has experienced massive and prolonged droughts over the last decade (Wang et al. 2015, 2018). Droughts in Southwest China rank among the most extreme in the world over the past decade (Orlowsky and Seneviratne, 2013), and receive widespread attention from both the government and academic sectors in China. All these drought events resulted in crop failure, lack of drinking water, ecosystem destruction, health problems, and even deaths (Qiu, 2010). Thus, it is meaningful to choose Southwest China as a research case.

2 Data

The monthly precipitation dataset used to carry out the case study over Southwest China has 0.5° × 0.5° horizontal grids and covers the period from 1961 to 2011. This dataset is elaborated by the National Meteorological Information Center of the China Meteorological Administration and is created based on 2474 ground observatories in China that have been subjected to rigorous quality control. A digital elevation model is introduced in the process of interpolation to take topographic effects into account.

In parallel, global monthly mean precipitation data are retrieved from the Global Precipitation Climatology Project (GPCP) (Adler et al. 2003), which is established and managed by the Global Energy and Water Cycle Experiment (GEWEX). This is a merged analysis that combines rain gauge data from more than 6000 stations worldwide and various satellite-based estimates of precipitation. The GPCP produces the best known and widely used global precipitation data in the meteorological community, covering the period from 1979 to 2011 at a horizontal resolution of 2.5°. Even though the GPCP data have global coverage, ocean data are excluded from the analyses and only global land data are utilized, since drought and its related impacts over land are of primary concern.

3 Methodology

3.1 Wavelet decomposition

Wavelet decomposition (WD), also called multiresolution analysis, is capable of decomposing a time series into several components, each of which is associated with a particular time scale. The WD concept and realization were initiated by Mallat (1989) and Meyer and Salinger (1995), and WD has found frequent application in signal processes and applied mathematics. Here, only a brief description of WD is presented; detailed information can be found in "Ten Lectures on Wavelets" (Daubechies 1992).

The formal definition of WD of $L^2(\mathbb{R})$ is a collection of successive closed subspaces $\{V_j\}_{j\in\mathbb{Z}}$ of $L^2(\mathbb{R})$ satisfying

$$
\begin{aligned}
&V_j \subset V_{j-1} \\
&\overline{\bigcup_{j\in\mathbb{Z}} V_j} = L^2(\mathbb{R}) \\
&\bigcap_{j\in\mathbb{Z}} V_j = \{0\} \\
&f \in V_j \Leftrightarrow f(2\cdot) \in V_{j-1} \\
&\textit{There exists } \phi \in V_0 \textit{ such that } \{\phi(\cdot - k), k \in \mathbb{Z}\} \textit{ is orthonormal basis for } V_0
\end{aligned}
\tag{1}
$$

In wavelet decomposition, ϕ is often called the "scaling function." Let $\phi_{j,\,k}(x) = 2^{-j/2}\phi(2^{-j}x - k)$; condition (1) implies that $\{\phi_{j,\,k}, k \in \mathbb{Z}\}$ is an orthonormal basis that spans V_j for all $j \in \mathbb{Z}$. Defining W_j to be the orthogonal complement of V_j in V_{j-1}, they are related by

$$V_{j-1} = V_j \oplus W_j \tag{2}$$

The vector space V_{j-1} is a linear combination of the "smooth" subspace V_j and the "detailed" subspace W_j. The basic theorem of multiresolution analysis is that when a sequence of closed subspaces satisfies condition (1), there exists $\{\psi_{i,\,j}(x) = 2^{-j/2}\psi(2^{-j}x - k), k \in \mathbb{Z}\}$, in which $\psi_{i,\,j}$ is generated by the translation and dilation of the "wavelet function" ψ, which forms the orthonormal basis of subspace W_j.

In the case of discrete time series, space V_0 has the finest resolution and contains the original data. Therefore, the projection of the data onto $\{V_j, j = 1, 2, 3\ldots\}$ has increasingly coarser resolution. Starting with V_0, the decomposition process at increasingly coarser resolution can be applied recursively, which can be expressed as

$$
\begin{aligned}
V_0 &= V_1 \oplus W_1 \\
&= V_2 \oplus W_2 \oplus W_1 \\
&= V_3 \oplus W_3 \oplus W_2 \oplus W_1 \\
&= \ldots
\end{aligned}
\tag{3}
$$

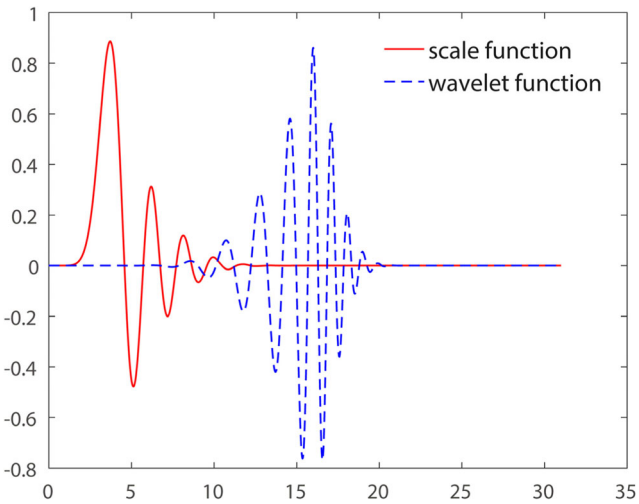

Fig. 1 Daubechies scaling (solid red line) and wavelet function (dashed blue line)

Data projected onto V_j is referred to as the decomposition of data at level j. Therefore, the wavelet decomposition of the signal at level j comprises the hierarchy of detailed information (W_1 to W_j) and the coarsest smoothing representation (V_j).

In practice, we need to choose the scaling function ϕ, wavelet function ψ, and maximum level of decomposition j. In this study, Daubechies scaling and wavelet functions as shown in Fig. 1 are chosen to perform decomposition and the maximum decomposition level is 5.

3.2 Standardized precipitation index

The Standardized Precipitation Index (SPI), as first introduced by McKee et al. (1993), is an effective tool for identifying the severity and period of droughts at multiple time scales. A detailed and clear description of the steps required to calculate the SPI is provided in Edwards and McKee (1997). The computation of the SPI is based on predefined time scales N, which correspond to the past n months of precipitation totals. The procedure consists of two main steps: first, a cumulative series is created at the desired time scale; second, the resultant data are fitted to the two-parameter Gamma distribution and then transformed into a normal distribution. The climatic classification according to the SPI is shown in Table 1. Because the time scale obtained by wavelet decomposition can only be a power of 2, the SPI is accordingly calculated at time scales of 2^0, 2^1, 2^2, 2^3, 2^4, and 2^5 months. Hereafter, P-n and SPI-n are referred to as the precipitation and SPI at a time scale of n months, respectively.

Table 1 Drought classifications according to SPI values

SPI value	Category
SPI ≥ 2.00	Extremely wet
1.50 ≤ SPI < 2.00	Very wet
1.00 ≤ SPI < 1.50	Moderately wet
− 1.00 ≤ SPI < 1.00	Near normal
− 1.50 ≤ SPI < − 1.00	Moderate drought
− 2.00 ≤ SPI < − 1.50	Severe drought
SPI ≤ − 2.00	Extreme drought

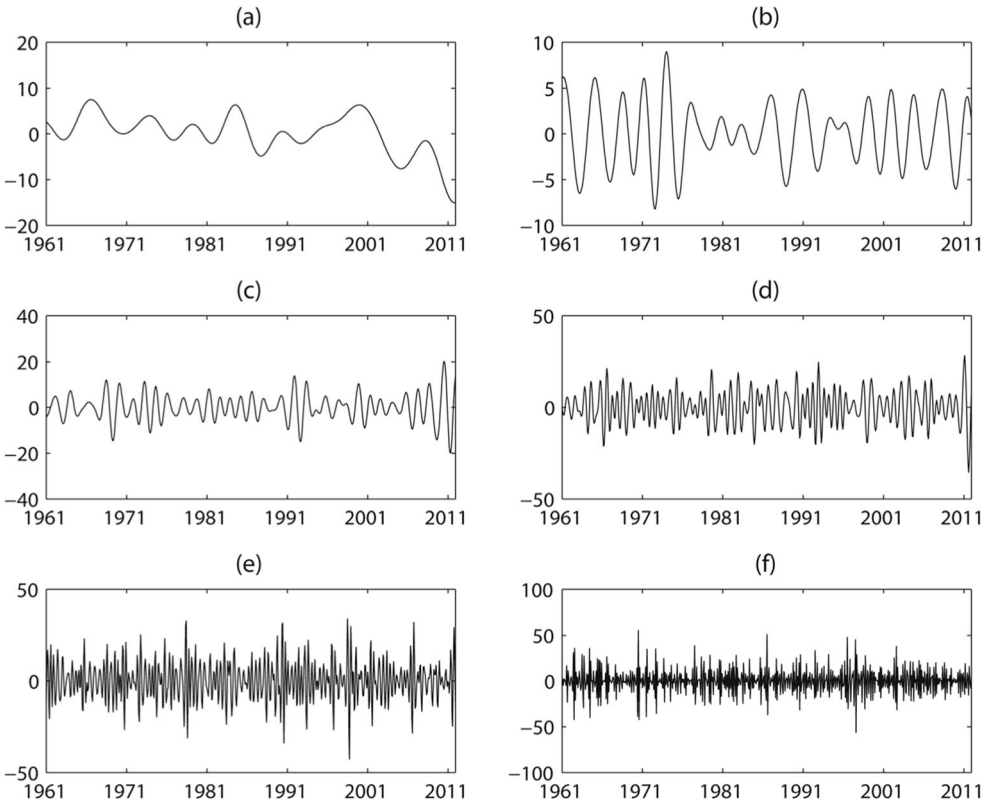

Fig. 2 The six components of the precipitation series over Southwest China at time scales of 2^5, 2^4, 2^3, 2^2, 2^1, and 2^0 months

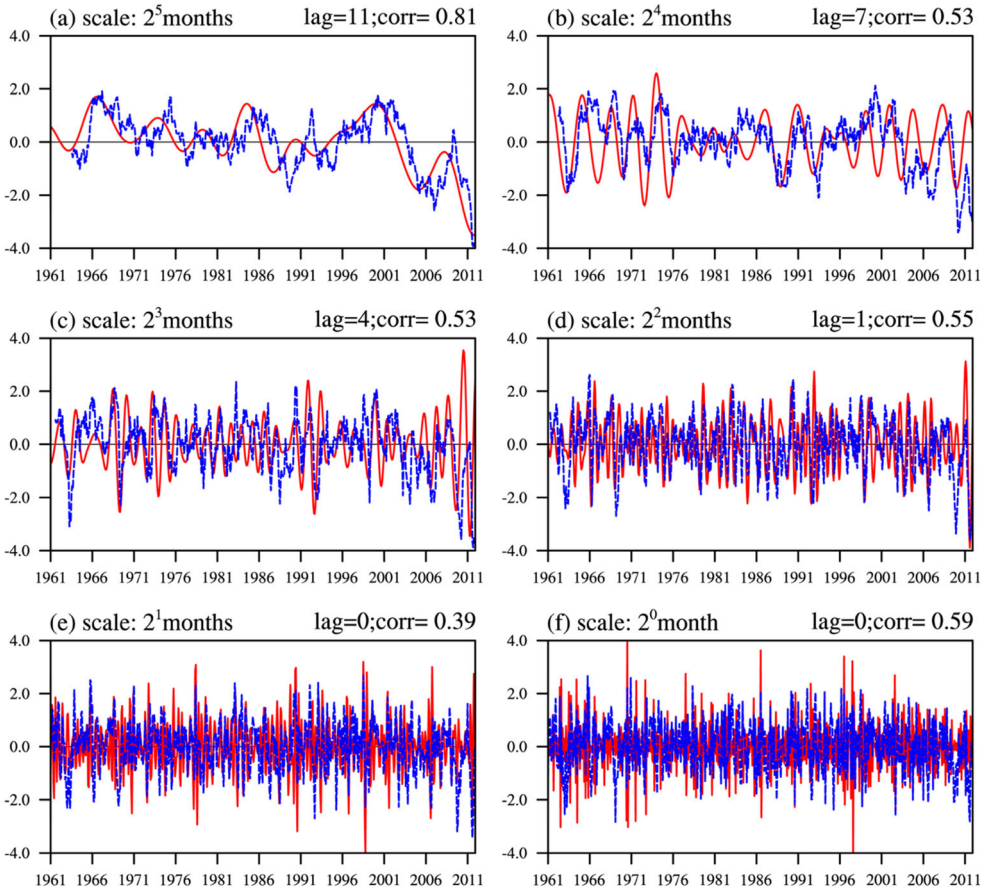

Fig. 3 Temporal variation of precipitation (solid red lines) and SPI (dashed blue lines) at time scales of 2^5, 2^4, 2^3, 2^2, 2^1, and 2^0 months. The maximum lagged correlation coefficient and its corresponding lag time are given at the top right in each subplot

4 A case study

This section aims to vividly illustrate the relationship between precipitation and the SPI, while a global analysis is described in Section 5. First, the annual cycle of the precipitation series over Southwest China is removed prior to wavelet decomposition. Second, the decomposition procedure is applied recursively, until the coarsest level of 5 is reached. Consequently, the multiresolution representation of the original data consists of the coarsest "smooth" representation at a time scale of 2^5 months (Fig. 2a), and the hierarchy of "detailed" components at time scales of 2^4, 2^3, 2^2, 2^1, and 2^0 months as shown in Fig. 2b–f. Figure 2 demonstrates that the amplitude and frequency steadily increase from longer time scales to shorter ones. The 2^5-month component appears to have interdecadal variability, with markedly long-term precipitation deficits in the last 10 years, which is in accordance with the massive and frequent drought events in Southwest China. In contrast, high-frequency oscillations with shorter duration are associated with shorter time scale variability.

The quantitative relationship between precipitation and the SPI at multiple time scales is examined by finding the lag that results in the maximum time-lagged correlation, as shown in Fig. 3. The time lag denotes how quickly the droughts at a specific time scale respond to precipitation anomalies. In fact, as shown below, the drought and corresponding index have a synchronous or delayed response to precipitation, depending on the time scale. At the time scale of 2^5 months, a positive lag of 11 months is identified, coupled with a maximum correlation of 0.8, indicating that the response time from the precipitation surplus or deficit to a rise or fall in the 32-month SPI indicative of hydrological wetness/dryness is 11 months. This phenomenon can be ascribed mainly to the considerable memory or persistence characteristics of hydrological systems including streamflow, groundwater level, reservoir, and lake storage, etc. As seen from Fig. 3a–f sequentially, the decreases in time scale not surprisingly lead to a decrease in the time lag at which the two series have the highest correlation. In particular, there is no delay between precipitation and the SPI at time scales of both 2^0 and 2^1, because the short-term SPI is closely tied to soil moisture, which is greatly sensitive to precipitation behavior.

These two methods, wavelet decomposition and the SPI procedure, which are based on completely different mathematical principles, both successfully detect the essential characteristics of precipitation, since all the time-lagged correlations irrespective of time scales are significant at the 99% confidence level. As stated in numerous studies, drought is a multiscalar phenomenon. Furthermore, the multiscalar character of drought originates from the multistructural property of precipitation, each occurring at different time scales. Specifically, the variation in the dry/wet state as reflected by the drought index at a particular time scale is regulated predominantly by the subseries separated from original precipitation data at that scale and is virtually unperturbed by any other components.

Table 2 Variance contributions of the six precipitation components (%)

Time scale (months)	2^5	2^4	2^3	2^2	2^1	2^0
Variance contribution (%)	4.1	2.6	7.2	18.1	24.8	43.2

Table 2 shows the contribution (%) of each component to the total variance. Remember that the decomposed components are linearly independent, as illustrated in Expression 3, and the original series can be regenerated as a sum of them, so the variance contribution can be easily calculated as the ratio of the component variance to the total. Table 2 demonstrates that the dominant contribution to the total variance of precipitation comes from the short and intermediate temporal scale structures, with the proportion explained by the 2^0- to 2^2-month series accounting for 86.1%. Furthermore, the variance contributions drastically decrease as the time scale increases. Although the component of longer time scales adds a relatively minor contribution to the total variability, it is indispensable to the long-term drought phenomenon and cannot be neglected. To substantiate this, we use the precipitation component at the time scale of 2^5 months, and all other parts

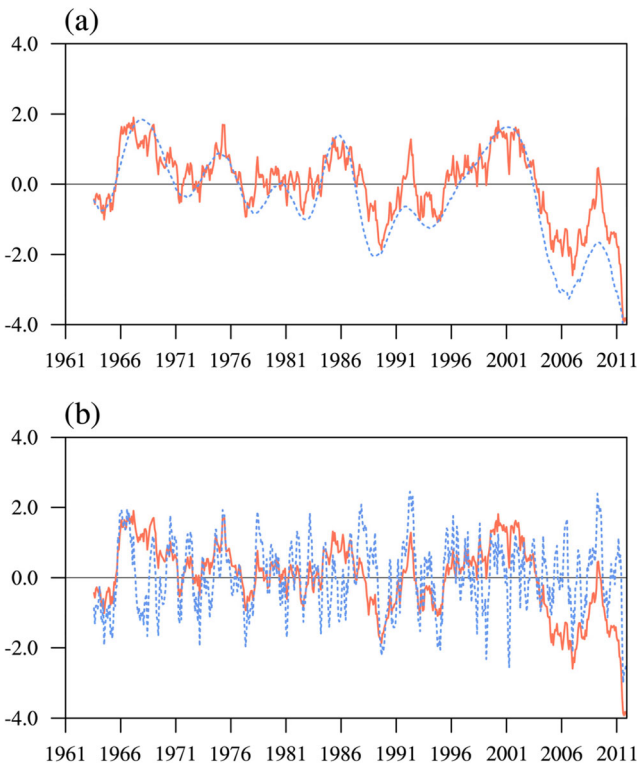

Fig. 4 Temporal variations in SPI constructed from the original precipitation data (solid red line), the component at the time scale of 2^5 months (dashed blue line in upper panel), and all the other components comprising the time scales ranging from 2^0 to 2^4 months (dashed blue line in bottom panel), respectively

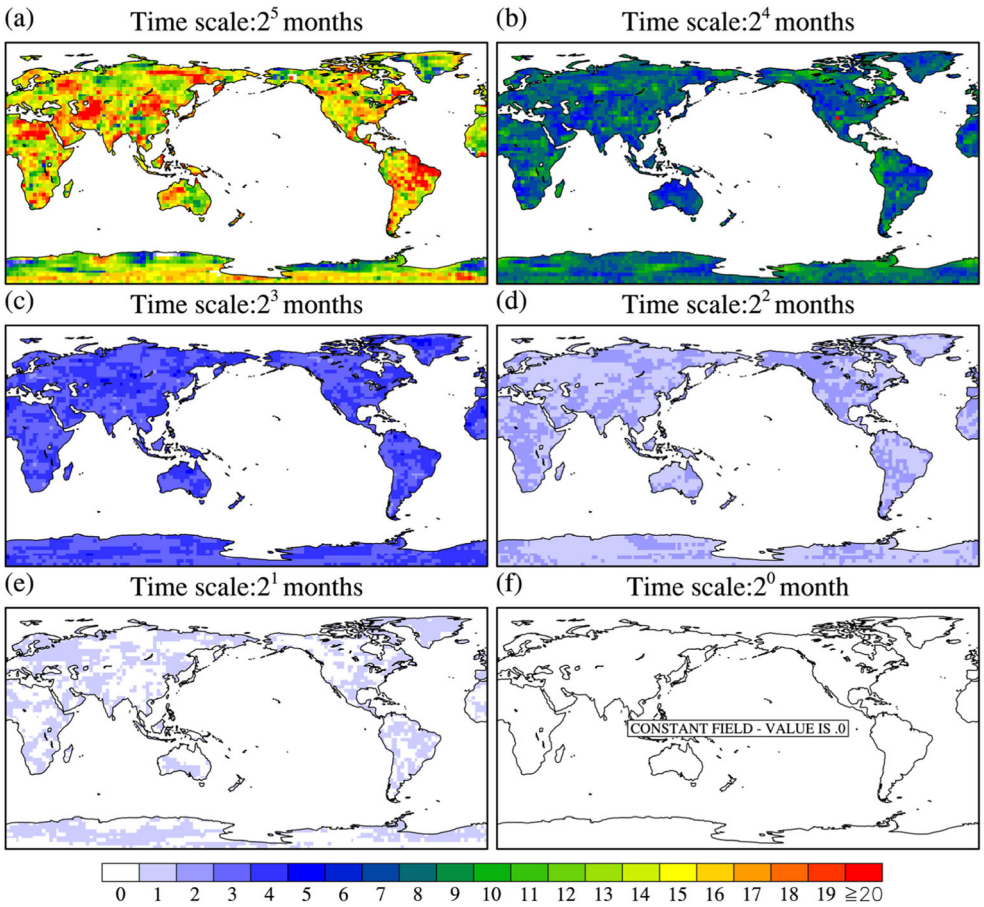

Fig. 5 Spatial distribution of the lag time between precipitation and the SPI at time scales of 2^5, 2^4, 2^3, 2^2, 2^1, and 2^0 months with the precipitation always leading the SPI

together whose variance contribution is 95.9%, to respectively construct the SPI series. The result depicted in Fig. 4 shows that the SPI-32 derived from the 2^5-month precipitation series perfectly resembles that calculated from the original data, with a simultaneous correlation coefficient of 0.92, while the SPI-32 induced from the precipitation excluding the 2^5-month component fails to match the actual pattern. For instance, the SPI series, computed from the aggregated components varying on time scales shorter than 2^4 months (Fig. 4b), demonstrates strong interannual variability without a significant trend in the last decade, which contradicts the observed reality of the negative values of the SPI-32 along with a persistent decreasing trend in this period. Consequently, it can be concluded that despite the very small contribution of the 2^5-month scale precipitation to the variance, to a great extent it determines the fluctuation of the SPI-32. This can be explained physically in that hydrological drought (long time scale), in terms of streamflow, ground water level, and so on, typically responds to the slowly varying (low frequency) component of precipitation and is insensitive to the components at shorter temporal scales, which have high-frequency oscillations.

Finally, it is necessary to stress that lag time and time scale are two completely different concepts. The time scale in the formulation of the SPI may lead to the misinterpretation that the time scale is equivalent to the time delay in the response of the SPI to precipitation. As seen in Fig. 3a, however, the 32-month SPI lags the 32-month precipitation by 11 months rather than 32 months. This can also be verified in Fig. 4a, in which the time series (dashed blue line) constructed from the 32-month precipitation leading the SPI by 11 months successfully reproduces the 32-month SPI (solid red line). Thus, the time scale reflects the behavior of the time series itself, while lag time refers to the time elapsed from the center of the excess/insufficient rainfall to the SPI peak/valley. This conclusion is further supported in the global analysis of the response-time lag, as discussed in Section 5.

5 Global analysis

In this section, the relationship between precipitation and the SPI is further investigated on a global scale. More specifically, the lag time in each grid cell is identified when the lagged correlation reaches its maximum. Therefore, a higher grid cell value denotes a longer response time of drought to a precipitation surplus or deficit. Figure 5 portrays the spatial patterns of lag time between precipitation and the SPI, with precipitation always leading the SPI. To provide a useful statistical description of the lag times worldwide, histograms are created

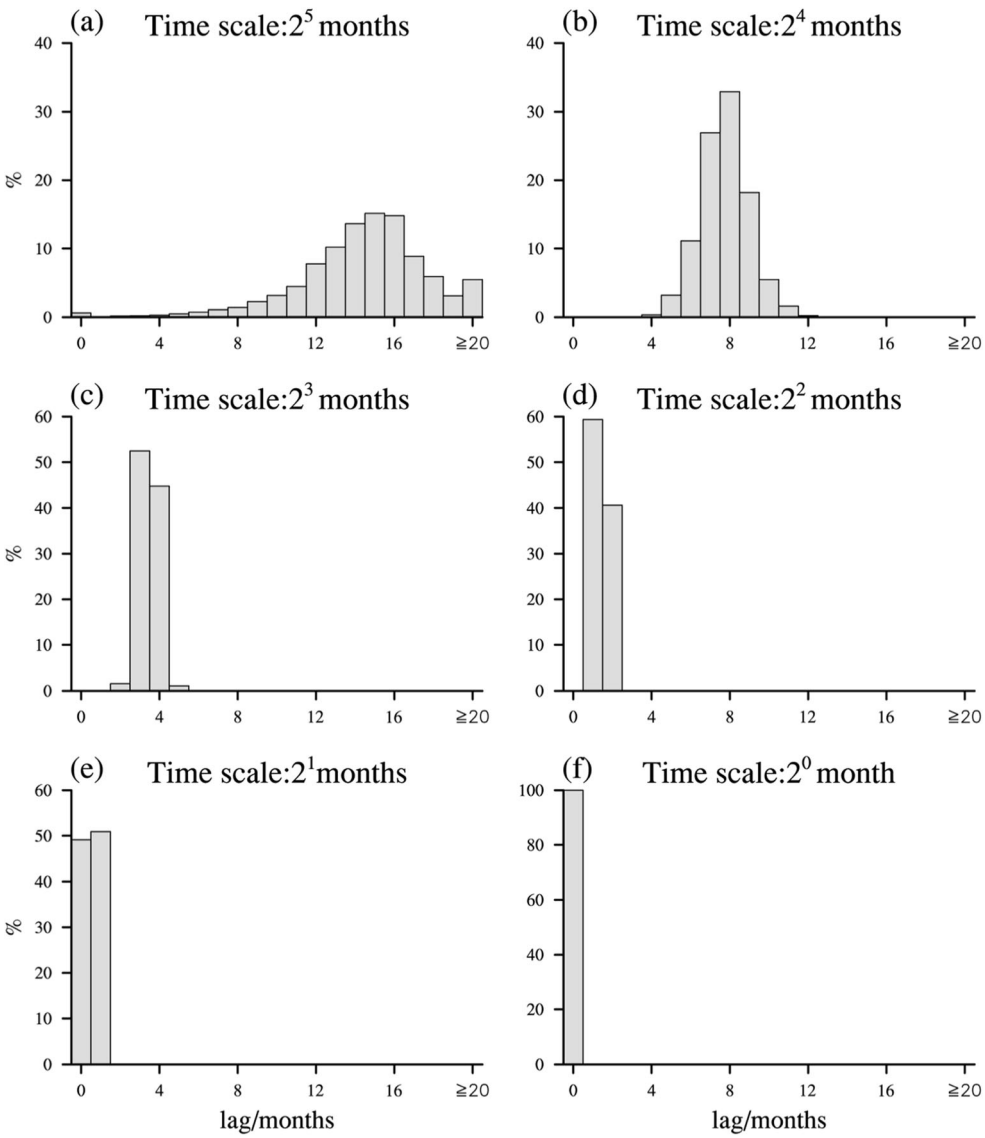

Fig. 6 Percent frequency distribution of global lag times between precipitation and the SPI. *x*- and *y*-coordinates denote the lag time and percentage of the total, respectively

in Fig. 6 to display the percentage of total grid cells falling in each of the time lags (0–19 months and ≥ 20 months).

Overall, the lag time between precipitation and the SPI gradually declines with the decrease in the time scale, as evidenced in both Figs. 5 and 6. It is also noteworthy that the percent distribution of time lags at longer time scales covers a wider range and is much less concentrated. At the time scale of 2^5 months, the delayed responses of the SPI-32 to P-32 have great geographic diversity, varying spatially from less than 10 months to a maximum of more than 20 months. This prominent feature can also be recognized in the percent frequency distribution as shown in Fig. 6a. North Africa, Central Asia, North China, and the Amazon basin appear to have a longer memory time (> 20 months), implying a considerable lag in the response of the dry/wet state to precipitation anomalies, while other locations are generally characterized by intermediate lag times (11–18 months). Because of the large spatial deviation, the distribution is broad and flat (Fig. 6a), with the peak probability being only 15.2% at lag = 15 months. However, lag times ranging from 11 to 18 months account for 76%, which indicates that the typical lag time between the SPI-32 and P-32 globally is in the narrower interval between 11 and 18 months. As the time scale decreases, the spatial discrepancies of lag time tend to diminish, and there is a more tightly clustered probability distribution. In particular, uniform lag times valued at 0 for the whole globe are observed at the time scale of 2^0 month, suggesting the synchronous response of the SPI to precipitation irrespective of location. From time scales of 2^4 to 2^1 months, the central value of lag time corresponding to peak probability continuously shifts to the left. At the time scale of 2^3 months, for example, the maximum correlation between precipitation and the SPI is achieved at a delay of 3 or 4 months, each of which contributes roughly half of all grid cells; when we move to time scales

of 2^2 and 2^1 months, a lag time of less than 2 months dominates over the globe.

As stated in Section 4, the concept of time lag is quite different from that of time scale. More precisely, as evidently illuminated in both Figs. 5 and 6, the lag time between precipitation and the SPI is commonly smaller than the time scale. At a time scale of 2^4 months, for example, the time lags are confined mainly between 7 and 9 months and never exceeds 12 months.

6 Conclusions and discussions

The main objective of this study is to provide a theoretical interpretation of multiscalar drought indices by examining the relationship between precipitation and the SPI. The SPI is multiscalar, enabling it to provide drought monitoring at different time scales. However, the multiple structures behind precipitation are not obvious and must first be identified. To this end, the wavelet decomposition technique is employed to decompose the precipitation into a number of orthogonal components according to different time scales.

A case study over Southwest China is first performed, which can offer additional detailed insights into this issue. Based on wavelet decomposition, the observed time series is composed of signals with different time scales. At the shorter time scales, on the one hand, the oscillation demonstrates a high frequency, short duration, and large amplitude; on the other hand, long duration and low frequency are observed at longer time scales. Precipitation and the SPI demonstrate a time-lagged relationship, with precipitation leading the SPI and the lag time being time-scale dependent. The longer the time scale, the more significant the delayed response of the SPI to precipitation, which is typically associated with hydrological parameters. In contrast, the shorter scale SPI, related to soil moisture and agricultural stress, exhibits an instantaneous reaction to precipitation behavior, with little or no delay. Most importantly, the SPI at a specific time responds almost exclusively to the corresponding precipitation component, despite the contribution of its variance to the total variability. In addition, two core concepts that are easily confused are clarified: time scale and lag time. The former is tied to the behavior of the time series itself, while the latter refers to the time between the peak rainfall and the peak in the SPI.

The global response time of the SPI to precipitation is then explored, further verifying and strengthening the conclusions from the case study. Moreover, we find that the magnitude of the lag time is highly site specific at longer time scales, ranging from 10 months to more than 20 months. In contrast, shorter time scales result in a spatially homogeneous distribution of lag time around the globe.

Finally, we would like to comment on researches related to drought indices. Recently, there has been a debate over which drought index is superior (Dai 2011b; Vicente-Serrano et al. 2011b). Our study reveals that the multiscalar nature of drought, as emphasized in many studies (Guttman 1999; Hayes et al. 1999; Khan et al. 2008), actually originates from the multistructural property hidden in precipitation variation, so that multiscalar drought indices such as the SPI are more suitable for detecting drought at a wide range of time scales than are other metrics with fixed time scales. In other words, a multiscalar drought index is a true reflection of the internal essence of precipitation variability. In fact, the SPI is now accepted by the World Meteorological Organization (WMO) as the universal meteorological drought index for more effective drought monitoring and early warning (Hayes et al. 2011). The results in this study favorably support the recommendations outlined in the "Lincoln Declaration on Drought Indices." In addition to the SPI, the SPEI, which is based on the mathematical principle of the SPI and thus inherits its versatility but also incorporates the influence of potential evaporation on drought, is also highly recommended. Recently, Wang et al. (2016) integrate SPEI at multiple time scales into a new metric called Comprehensive Multiscalar Indicator (CMI) that is specifically designed for super drought detection. Therefore, the collaborative use of SPEI and CMI can provide understanding and monitoring drought phenomenon.

Acknowledgments We thank Prof. Wen Zhou (City University of Hong Kong) for a useful discussion during the course of this work. The editor and anonymous reviewers provide constructive comments and suggestions which improve the quality of this paper. Also, we are grateful to the China Meteorological Data Service Center for providing the precipitation data in China, as well as the NOAA/OAR/ESRL PSD for publicly sharing the GPCP data.

Funding information This research was supported by the National Natural Science Foundation of China Grant Nos. 41661144016 and 41505069, Public science and technology research funds projects of ocean Grant No. 201505013, and Open Research Fund Program of Plateau Atmosphere and Environment Key Laboratory of Sichuan Province Project No. PAEKL-2018-C1.

References

Adler RF, Huffman GJ, Chang A, Ferraro R, Xie PP, Janowiak J, Rudolf B, Schneider U, Curtis S, Bolvin D (2003) The version-2 global precipitation climatology project (GPCP) monthly precipitation analysis (1979-present). J Hydrometeorol 4(6):1147–1167

Dai A (2011a) Drought under global warming: a review. Wiley Interdiscip Rev Clim Chang 2:45–65

Dai A (2011b) Characteristics and trends in various forms of the palmer drought severity index during 1900-2008. J Geophys Res 116(D12): D12115

Daubechies I (1992) Ten lectures on wavelets. Cambridge University Press, Cambridge, U. K.

Edwards DC, McKee TB (1997) Characteristics of 20th century drought in the United States at multiple time scales. Atmos Sci pap 634, Colorado state Univ, Fort Collins

Guttman NB (1998) Comparing the palmer drought index and the standardized precipitation index. J Am Water Resour Assoc 34:113–121

Guttman NB (1999) Accepting the standardized precipitation index: a calculation algorithm. J Am Water Resour Assoc 35:311–322

Hayes MJ, Svoboda MD, Wilhite DA, Vanyarkho OV (1999) Monitoring the 1996 drought using the standardized precipitation index. Bull Am Meteorol Soc 80(3):429–438

Hayes M, Svoboda M, Wall N, Widhalm M (2011) The Lincoln declaration on drought indices: universal meteorological drought index recommended. Bull Am Meteorol Soc 92:485–488

Heim RR (2000) Drought indices: a review. in *Drought: A Global Assessment*, hazards disasters Ser., vol. I, edited by D. A. Wilhite, pp. 159–167, Routledge, New York

Heim RR (2002) A review of twentieth-century drought indices used in the United States. Bull Am Meteorol Soc 83:1149–1165

Khan S, Gabriel H, Rana T (2008) Standard precipitation index to track drought and assess impact of rainfall on watertables in irrigation areas. Irrig Drainage Syst 22(2):159–177

Mallat SG (1989) A theory for multiresolution signal decomposition: the wavelet representation. Pattern Analysis and Machine Intelligence, IEEE Transactions on 11(7):674–693

McEvoy DJ, Huntington JL, Abatzoglou J, Edwards L (2012) An evaluation of multiscalar drought indices in Nevada and eastern California. Earth Interact 16:1–8

McKee TB, Doesken NJ, Kleist J (1993) The relationship of drought frequency and duration to time scales, preprints, 8th Conf. On applied climatology, Anaheim, CA, Amer. Meteor. Soc., 179–184

McKee TB, Doesken NJ, Kleist J (1995) Drought monitoring with multiple time scales, preprints, 9th Conf. On applied climatology, Dallas, TX, Amer. Meteor. Soc., 233–236

Meyer Y, Salinger DH (1995), Wavelets and operators, Cambridge University Press

Meyers SD, Kelly BG, O'Brian JJ (1993) An introduction to wavelet analysis in oceanography and meteorology: with application to the dispersion of Yanai waves. Mon Wea Rev 121:2858–2866

Orlowsky B, Seneviratne SI (2013) Elusive drought: uncertainty in observed trends and short- and long-term CMIP5 projections. Hydrol Earth Syst Sci 17(5):1765–1781

Palmer WC (1965) Meteorological drought. U.S. Department of Commerce research paper 45, pp. 58

Qiu J (2010) China drought highlights future climate threats. Nature 465: 142–143

Torrence C, Compo GP (1998) A practical guide to wavelet analysis. Bull Am Meteorol Soc 79(1):61–78

Vicente-Serrano SM, Beguería D, López-Moreno JI (2010) A multiscalar drought index sensitive to global warming: the standardized precipitation evapotranspiration index. J Clim 23(7):1696–1718

Vicente-Serrano SM, López-Moreno JI, Drumond S, Gimeno L, Nieto R, Morán-Tejeda E, Lorenzo-Lacruz J, Beguería S, Zabalza J (2011a) Effects of warming processes on droughts and water resources in the NW Iberian Peninsula. Clim Res 48(2–3):203–212

Vicente-Serrano SM, Beguería S, López-Moreno JI (2011b) Comment on "characteristics and trends in various forms of the palmer drought severity index (PDSI) during 1900-2008" by Aiguo Dai. J Geophys Res 116(D19):D19112

Vicente-Serrano SM, Beguería D, Lorenzo-Lacruz J, Camarero JJ, López-Moreno JI, Azorin-Molina C, Revuelto J, Morán-Tejeda E, Sánchez-Lorenzo A (2012) Performance of drought indices for ecological, agricultural and hydrological applications. Earth Interact 16(10):1–27

Wang L, Chen W (2014) Applicability analysis of standardized precipitation evapotranspiration index in drought monitoring in China. Plateau Meteorology 33(2):423–431 (in Chinese)

Wang L, Chen W, Zhou W, Huang G (2015) Drought in Southwest China: a review. Atmos Oceanic Sci Lett 8(6):339–344

Wang L, Chen W, Zhou W, Huang G (2016) Understanding and detecting super extreme droughts in Southwest China through an integrated approach and index. Q J R Meteorol Soc 142(694):529–535

Wang L, Huang G, Chen W, Zhou W, Wang W (2018) Wet-to-dry shift over Southwest China in 1994 tied to the warming of tropical warm pool. Clim Dyn, https://doi.org/10.1007/s00382-018-4068-8

Wells N, Goddard S, Hayes MJ (2004) A self-calibrating palmer drought severity index. J Clim 17(12):2335–2351

Wilhite DA (2000) Drought as a natural hazard: concepts and definitions, in *Drought: A Global Assessment, Hazards Disasters* Ser., vol. I, edited by D. A. Wilhite, pp. 3–18, Routledge, New York

Wilhite D A (2006) Drought monitoring and early warning: concepts, progress and future challenges, *WMO*-no. 1006, World Meteorological Organization, Geneva, Switzerland